Predominant role of endothelial nitric oxide synthase in vascular endothelial growth factor-induced angiogenesis and vascular permeability

Dai Fukumura*†, Takeshi Gohongi*, Ananth Kadambi*, Yotaro Izumi*, Jennifer Ang*, Chae-Ok Yun*, Donald G. Buerk‡, Paul L. Huang§, and Rakesh K. Jain*

*Edwin L. Steele Laboratory and Department of Radiation Oncology, §Cardiovascular Research Center and Department of Medicine, Massachusetts General Hospital and Harvard Medical School, Boston, MA 02114; and ‡Departments of Physiology and Bioengineering, University of Pennsylvania School of Medicine, Philadelphia, PA 19104

Edited by Louis J. Ignarro, University of California, Los Angeles, CA, and approved December 13, 2000 (received for review July 31, 2000)

Nitric oxide (NO) plays a critical role in vascular endothelial growth factor (VEGF)-induced angiogenesis and vascular hyperpermeability. However, the relative contribution of different NO synthase (NOS) isoforms to these processes is not known. Here, we evaluated the relative contributions of endothelial and inducible NOS (eNOS and iNOS, respectively) to angiogenesis and permeability of VEGF-induced angiogenic vessels. The contribution of eNOS was assessed by using an *eNOS*-deficient mouse, and iNOS contribution was assessed by using a selective inhibitor [L-N^6-(1-iminoethyl) lysine, L-NIL] and an *iNOS*-deficient mouse. Angiogenesis was induced by VEGF in type I collagen gels placed in the mouse cranial window. Angiogenesis, vessel diameter, blood flow rate, and vascular permeability were proportional to NO levels measured with microelectrodes: Wild-type (WT) ≥ WT with L-NIL or $iNOS^{-/-}$ > $eNOS^{-/-}$ ≥ $eNOS^{-/-}$ with L-NIL. The role of NOS in VEGF-induced acute vascular permeability increase in quiescent vessels also was determined by using *eNOS*- and *iNOS*-deficient mice. VEGF superfusion significantly increased permeability in both WT and $iNOS^{-/-}$ mice but not in $eNOS^{-/-}$ mice. These findings suggest that eNOS plays a predominant role in VEGF-induced angiogenesis and vascular permeability. Thus, selective modulation of eNOS activity is a promising strategy for altering angiogenesis and vascular permeability *in vivo*.

Vascular endothelial growth factor (VEGF) is a potent angiogenic and vascular permeabilizing factor (1, 2). VEGF plays a critical role in both physiological and pathological angiogenesis. Nitric oxide (NO) is known to mediate many physiological and pathological functions, including angiogenesis and vascular permeability (3–7). There are three isoforms of NO synthase (NOS): neuronal NOS (nNOS, also referred to as type I NOS), inducible NOS (iNOS, type II NOS), and endothelial NOS (eNOS, type III NOS). These three isoforms of NOS are distributed and regulated differently (8). VEGF promotes NO production and also induces eNOS and iNOS expression in vascular endothelial cells *in vitro* (9–11). Furthermore, inhibition of *in vivo* NO production results in reduced angiogenesis and vascular permeability induced by VEGF (12, 13). However, the relative contribution of the individual isoforms of NOS and the absolute amount of NO involved in these different functions *in vivo* are not known. Thus, in this study, we evaluated the relative contributions of eNOS and iNOS in VEGF-induced angiogenesis and vascular permeability using a collagen gel quantitative angiogenesis assay and *eNOS*- and *iNOS*-deficient mice as well as the iNOS selective inhibitor L-N^6-(1-iminoethyl) lysine (L-NIL).

Methods

Animals. To obtain mice with an immunodeficient background, we crossed $eNOS^{-/-}$ mice (14) with recombination activating gene 1 null ($Rag\text{-}1^{-/-}$) mice (The Jackson Laboratory). $Rag\text{-}1^{-/-}$ mice lack mature T and B cells (15). The response in the double knockout mice, homozygous for both the *eNOS* gene and the *Rag-1* gene ($eNOS^{-/-}Rag\text{-}1^{-/-}$) was compared with that in $eNOS^{+/+}Rag\text{-}1^{-/-}$ mice [referred to wild-type (WT) $Rag\text{-}1^{-/-}$, WT mice for *eNOS* gene]. These mice had mixed C57BL/6 and SV129 background. Separate immunocompetent animals were used for acute vascular permeability, pial vessel hemodynamic studies, and angiogenesis assay for *iNOS*-deficient mice: $iNOS^{-/-}$ mice backcrossed for 10 generations to C57BL/6 background (The Jackson Laboratory), C57BL/6 WT animals, and $eNOS^{-/-}$ mice backcrossed for 10 generations to C57BL/6 background. Both males and females of all genotypes of mice were kept in the barrier animal facility in Massachusetts General Hospital under diurnal lighting conditions and allowed free access to food and water. All procedures were carried out following Institutional Animal Care and Use Committee approval.

Angiogenesis Assay. Angiogenesis in type I collagen gel was monitored as described (16, 17). In brief, immunodeficient mice were anesthetized (90 mg/kg Ketamine and 9 mg/kg Xylazine) and implanted with cranial windows. Seven to 10 days later, the coverslip was removed, and type I collagen gel (20 μl) containing VEGF-165 (3 μg/ml, R&D Systems, Minneapolis, MN) sandwiched between nylon meshes (2.5 × 2.5 mm) was inoculated onto the pial surface. The cranial window was then closed with a glass coverslip. Angiogenic vessels in the gel were noninvasively monitored daily for 14 days. Angiogenesis was quantified as a percentage of squares in the top nylon mesh containing at least one vessel. The time required to fill 50% of squares in the mesh (A_{50}) also was determined from the individual angiogenic response curves. Rate of angiogenesis (A_{Rate}) was then calculated as follows: A_{Rate} (%/day) = 50 (%)/A_{50} (day).

Intravital Microscopy. To obtain physiological parameters of the angiogenic vessels, 4–5 randomly selected locations of the gel were investigated by intravital fluorescence microscopy on day 14 after the gel implantation as described (16–18). Briefly, FITC-labeled dextran (molecular weight, 2,000,000; 10 mg/ml, 100 μl, Sigma) was injected into the animal's tail vein to enhance contrast between red blood cells (RBCs) and plasma. For functional vessel density, the total length of perfused microvessels per unit area was measured. Vessel diameter was measured

This paper was submitted directly (Track II) to the PNAS office.

Abbreviations: VEGF, vascular endothelial growth factor; NOS, NO synthase; nNOS, neuronal NOS; iNOS, inducible NOS; eNOS, endothelial NOS; *Rag-1*, recombination activating gene 1; L-NIL, L-N^6-(1-iminoethyl) lysine; WT, wild type; RBC, red blood cell.

†To whom reprint requests should be addressed at: Massachusetts General Hospital, 100 Blossom Street, Boston, MA 02114. E-mail: dai@steele.mgh.harvard.edu.

The publication costs of this article were defrayed in part by page charge payment. This article must therefore be hereby marked "*advertisement*" in accordance with 18 U.S.C. §1734 solely to indicate this fact.

www.pnas.org/cgi/doi/10.1073/pnas.041359198

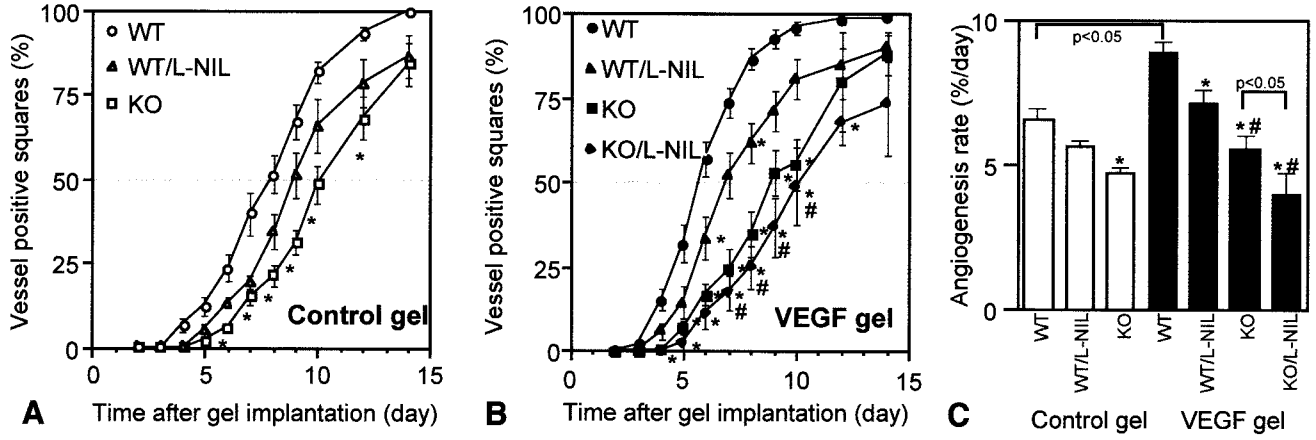

Fig. 1. Angiogenesis in collagen gels. Angiogenesis in control collagen gels (*A*) and VEGF (3 μg/ml) containing gels (*B*) in mouse cranial window was monitored for 14 days. Angiogenesis was quantified as the percentage of squares in the top nylon mesh containing at least one vessel. (*A*) In the control gels, *eNOS*$^{-/-}$*Rag-1*$^{-/-}$ mice (□ KO, $n = 10$) showed significantly reduced angiogenesis compared with WT *Rag-1*$^{-/-}$ (○, $n = 10$) mice. L-NIL (an iNOS selective inhibitor)-treated *Rag-1*$^{-/-}$ mice (△ WT/L-NIL, $n = 4$) showed slightly slower angiogenesis than WT/control but the difference was not significant at any time point. (*B*) In the VEGF gel, L-NIL treatment (▲ WT/L-NIL, $n = 8$) modestly reduced angiogenesis ($P < 0.05$ compared with nontreated *Rag-1*$^{-/-}$ mice at day 6 and day 8). Angiogenesis in *eNOS*$^{-/-}$*Rag-1*$^{-/-}$ mice (■ KO, $n = 15$) was significantly reduced compared with *Rag-1*$^{-/-}$ mice (● WT, $n = 16$). L-NIL treatment of *eNOS*$^{-/-}$*Rag-1*$^{-/-}$ mice (◆ KO/L-NIL, $n = 6$) further delayed angiogenesis. (*C*) The rate of angiogenesis was calculated from time required to fill 50% of squares in the mesh, which is derived from individual angiogenic response curves (*A* and *B*). VEGF (3 ng/μl) significantly accelerated angiogenesis in *Rag-1*$^{-/-}$ (WT) mice with or without L-NIL treatment, but not in *eNOS*$^{-/-}$*Rag-1*$^{-/-}$ (KO) mice. In both control gel and VEGF gel, L-NIL treatment slightly slowed the angiogenesis and KO showed significantly slower angiogenesis than WT mice. Inhibition of both eNOS and iNOS (KO/L-NIL) resulted in further delays in angiogenesis. *, $P < 0.05$ as compared with WT mice. #, $P < 0.05$ as compared with WT mice with L-NIL treatment.

by using an image-shearing device, and RBC velocity was measured by temporal correlation velocimetry. The blood flow rate of individual vessels was calculated by using vessel diameter and RBC velocity (18). The effective vascular permeability coefficient was measured as described (18) using tetramethylrhodamine-labeled BSA (10 mg/ml, 100 μl, Molecular Probes).

iNOS Inhibitor Treatment. Both WT *Rag-1*$^{-/-}$ and *Rag-1*$^{-/-}$*eNOS*$^{-/-}$ mice were treated with either L-NIL, a selective type II NOS inhibitor (Alexis Biochemicals, San Diego) (19) or vehicle. The treatment started 1 day before the collagen gel implantation and continued until the end of the observation period. The IC_{50} of L-NIL for mouse iNOS is 3.7 μM (20). For *in vivo* use, we followed the protocol of Stenger *et al.* (19) and treated animals with 4.5 mM L-NIL in drinking water. With the same treatment, a 21-fold reduction in NOS activity was observed in the lymph nodes of chronically infected mice (19).

VEGF Superfusion. To study the role of NOS in VEGF-induced acute permeability increase, dorsal skin chambers in immunocompetent C57BL/6, *eNOS*$^{-/-}$, and *iNOS*$^{-/-}$ mice were superfused with VEGF-165 (50 ng/ml, 20 μl) as described (21). Dorsal skin chambers were used in this experiment because normal pial vessels require a several order higher pharmacological concentration of VEGF to increase vascular permeability acutely (21). Briefly, baseline vascular permeability after PBS superfusion was measured by using either tetramethylrhodamine or cyanine 5-(Amersham Pharmacia) labeled BSA. Twenty to 40 minutes after VEGF superfusion, vascular permeability to BSA labeled with the alternate fluorescent tracer was measured.

NO Measurement. NO was measured in the gel and underlying cortex by a polarographic electrochemical method using recessed Nafion-polymer-coated gold microsensors (see supplemental material, which is published on the PNAS web site, www.pnas.org) (22). After the cranial window was opened, the brain was immediately covered with saline. A stainless steel ring superfusion well was cemented to the skull, and the animal was immobilized in a head holder. The well over the brain was superfused with Earle's balanced salt solution (Sigma) equilibrated with 5% O_2, 5% CO_2, balance N_2 and maintained at 37°C by a circulating water bath. The pH in the buffer under these conditions was 7.1 ± 0.02 ($n = 6$, mean ± SD). A Ag/AgCl reference electrode was placed into the well. NO microsensors were positioned at a 45° angle with a micromanipulator. NO microsensors were advanced into the gel at a rate of ≈240 μm/min using a hydraulic microdrive (Kopf Instruments, Tujunga, CA). The penetration was started ≈200 μm above the gel surface. Penetrations were observed under a microscope, and terminated if any bending of the NO microsensor was seen. A data point was obtained for every 1-μm advancement of the NO microsensor. After advancing the electrode through the gel and into the underlying cortex, the penetration was stopped and the NO microsensor was rapidly withdrawn back to a position in the well ≈500 μm above the gel surface. NO profiles across the gel are displayed with respect to the vertical depth from the surface, correcting for the angle of penetration, with mean ± SEM for each 50-μm increment.

Statistics. The data were analyzed by using an ANOVA and the Fisher's post hoc test unless otherwise specified. Values are expressed as mean ± SEM unless otherwise specified. Statistical significance was set at $P < 0.05$.

Results

Angiogenesis Is Significantly Reduced in *eNOS*$^{-/-}$*Rag-1*$^{-/-}$ Mice. We quantified angiogenesis in immunodeficient mice by using a recently developed collagen gel model (16). This model provides highly reproducible, quantitative information about temporal changes in vascularization *in vivo*. All mice used had a *Rag-1*$^{-/-}$ background. The involvement of eNOS or iNOS in this process was evaluated by using *eNOS*-deficient mice or the iNOS selective inhibitor L-NIL. After implantation of the control collagen gels (without exogenous VEGF), *eNOS*$^{-/-}$*Rag-1*$^{-/-}$ mice showed significantly reduced angiogenesis compared with WT *Rag-1*$^{-/-}$ mice (Fig. 1*A*). The response of L-NIL-treated WT

Rag-1$^{-/-}$ mice fell between the response of these two groups.

In gels containing VEGF (3 μg/ml) in WT *Rag-1*$^{-/-}$ mice, angiogenesis was significantly accelerated compared with control gels with or without L-NIL treatment. Decreased vascularization in *eNOS*$^{-/-}$*Rag-1*$^{-/-}$ mice compared with WT *Rag-1*$^{-/-}$ mice was even more clearly visible in the VEGF gel (Fig. 1 *B* and *C*). Furthermore, VEGF did not change the rate of angiogenesis in *eNOS*$^{-/-}$*Rag-1*$^{-/-}$ mice (Fig. 1*C*). The iNOS inhibitor slightly slowed angiogenesis in WT *Rag-1*$^{-/-}$ mice, and there was an additive effect of L-NIL on decreased angiogenesis in *eNOS*$^{-/-}$*Rag-1*$^{-/-}$ mice. In summary, angiogenesis in VEGF gel decreased according to the following order: WT *Rag-1*$^{-/-}$ $\geq$ WT *Rag-1*$^{-/-}$ with L-NIL $>$ *eNOS*$^{-/-}$*Rag-1*$^{-/-}$ $\geq$ *eNOS*$^{-/-}$*Rag-1*$^{-/-}$ with L-NIL.

eNOS$^{-/-}$Rag-1$^{-/-}$ Mice Show Reduced Angiogenesis and Blood Flow. At 14 days after collagen gel implantation, we determined functional vascular density (total length of perfused vessels per unit area), vessel diameter, RBC velocity, and blood flow rate in angiogenic vessels by intravital microscopy. The *eNOS*$^{-/-}$*Rag-1*$^{-/-}$ mice exhibited significant reduction in vascular density compared with WT *Rag-1*$^{-/-}$ mice with or without L-NIL (Fig. 2). L-NIL treatment did not significantly change vascular densities in VEGF gels in either WT *Rag-1*$^{-/-}$ or *eNOS*$^{-/-}$*Rag-1*$^{-/-}$ mice. Changes in vessel diameter showed a pattern similar to angiogenesis rate: WT *Rag-1*$^{-/-}$ $\geq$ WT *Rag-1*$^{-/-}$ with L-NIL $\geq$ *eNOS*$^{-/-}$*Rag-1*$^{-/-}$ $\geq$ *eNOS*$^{-/-}$*Rag-1*$^{-/-}$ with L-NIL; however, the difference was not statistically significant ($P = 0.0573$, WT *Rag-1*$^{-/-}$ vs. *eNOS*$^{-/-}$*Rag-1*$^{-/-}$ with L-NIL). There was no difference in RBC velocity regardless of mouse genotype or treatment. The blood flow rate in individual vessels was reduced in *eNOS*$^{-/-}$*Rag-1*$^{-/-}$ mice ($P = 0.037$) compared with WT *Rag-1*$^{-/-}$ mice. Overall hemodynamics and functional vessel densities were consistent with an angiogenic response.

iNOS Plays Limited Role in Angiogenesis. To further confirm the involvement of iNOS in VEGF-induced angiogenesis, we repeated the angiogenesis gel assay using immunocompetent C57BL/6 mice and *iNOS*$^{-/-}$ mice with C57BL/6 background. Similar to L-NIL experiments, angiogenesis in *iNOS*$^{-/-}$ mice was slightly slower than C57BL/6 mice (Table 1 and Fig. 5, which is published as supplemental material). At 14 days after VEGF gel implantation, *iNOS*$^{-/-}$ mice showed significantly lower vessel density but comparable vessel diameter compared with C57BL/6 mice.

eNOS But Not iNOS Mediates VEGF-Induced Vascular Permeability Increase in Quiescent Vessels. To determine the involvement of eNOS and iNOS in VEGF-induced acute vascular permeability increase, we measured vascular permeability in mouse dorsal skin chambers after VEGF superfusion in immunocompetent *eNOS* and *iNOS* null mice. The baseline vascular permeability was comparable among *eNOS*$^{-/-}$, *iNOS*$^{-/-}$, and WT C57BL/6 mice (Fig. 3*A*). Immediately after VEGF superfusion, vascular permeability increased significantly in *iNOS*$^{-/-}$ and C57BL/6 mice but not in *eNOS*$^{-/-}$ mice (Fig. 3*A*). Twenty-four hours after the superfusion, vascular permeability returned to the baseline level (data not shown). Thus, VEGF-induced acute permeability increase in quiescent vessels was significantly inhibited in *eNOS*$^{-/-}$ mice.

eNOS Mediates Vascular Permeability in VEGF-Induced Angiogenic Vessels. Fourteen days after the collagen gel implantation, vascular permeability of newly formed vessels in VEGF gels in WT *Rag-1*$^{-/-}$ mice ($2.5 \pm 0.4 \times 10^{-7}$ cm/s) was significantly higher compared with the control gels in WT *Rag-1*$^{-/-}$ mice ($1.3 \pm 0.4 \times 10^{-7}$ cm/s, $P = 0.035$). NOS inhibition in the VEGF gels (WT *Rag-1*$^{-/-}$ with L-NIL, *eNOS*$^{-/-}$*Rag-1*$^{-/-}$, *eNOS*$^{-/-}$*Rag-1*$^{-/-}$ with L-NIL) resulted in decreased permeability ($1.6 \pm 0.3 \times 10^{-7}$ cm/s, $P = 0.0727$; $1.2 \pm 0.8 \times 10^{-7}$ cm/s, $P = 0.035$; $0.5 \pm 0.2 \times 10^{-7}$ cm/s, $P = 0.003$, respectively) (Fig. 3*B*). Vascular perme-

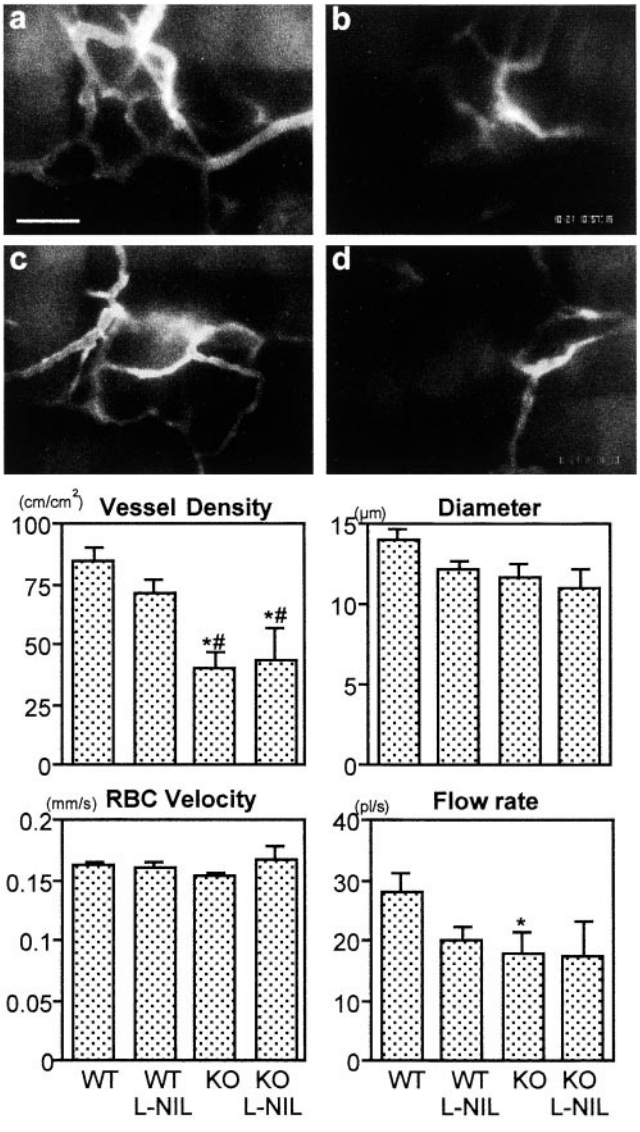

Fig. 2. Functional vessel density and hemodynamic parameters of angiogenic vessels in VEGF gels. At 14 days after collagen gel implantation, functional vessel density (defined as total length of perfused vessels per unit area), diameter, RBC velocity, and blood flow rate of angiogenic vessels were determined by intravital microscopy. Representative images of angiogenic vessels in VEGF gels (*a* and *b*) and VEGF gels with L-NIL treatment (*c* and *d*) at 14 days after implantation are shown. The vessel density in *eNOS*$^{-/-}$*Rag-1*$^{-/-}$ mice (*b* and *d*) was significantly reduced compared with that in *Rag-1*$^{-/-}$ mice (*a* and *c*). The area of each high-power image is roughly same as the size of one square of the mesh. The autofluorescence of nylon mesh can be seen at the top or left side of *a* and elsewhere. (Scale bar = 100 μm.) In the VEGF gel, *eNOS*$^{-/-}$*Rag-1*$^{-/-}$ mice (KO) showed significantly smaller vascular density compared with *Rag-1*$^{-/-}$ (WT) mice with or without L-NIL treatment. L-NIL treatment did not significantly change vascular density in VEGF gels in both WT and KO mice. Vessel diameter showed a trend similar to angiogenesis rate (Fig. 1), WT $>$ WT with L-NIL $>$ KO $>$ KO with L-NIL. However, there was no statistically significant difference ($P = 0.0573$, WT vs. KO with L-NIL). There was no difference in RBC velocity regardless of mice genotype and treatment. Blood flow rate in individual vessel was reduced in KO mice ($P = 0.037$) compared with WT mice. A total of 58 locations in 12 WT mice, 30 locations in six L-NIL-treated WT mice, 26 locations in five KO mice, and 15 locations in three L-NIL-treated KO mice were observed. *, $P < 0.05$ as compared with WT mice. #, $P < 0.05$ as compared with WT mice with L-NIL treatment.

Table 1. VEGF-induced angiogenesis and vascular permeability in *iNOS* mutant mice

Genotype	Angiogenesis rate, % per day	Vessel density,‡ cm/cm²	Vessel diameter,‡ μm	Vascular permeability, 10^{-7} cm/s
WT ($n = 10$)†	6.1 ± 0.2	67.0 ± 3.7	12.0 ± 0.3	4.4 ± 1.2
iNOS$^{-/-}$ ($n = 8$)†	5.5 ± 0.3	44.2 ± 6.0*	11.6 ± 0.4	4.1 ± 1.4

*, $P < 0.05$ as compared with WT.
†C57BL/6 single strain background.
‡Total of 50 and 40 locations were determined for WT and *iNOS*$^{-/-}$, respectively.

ability in angiogenic vessels in the immunodeficient *Rag-1*$^{-/-}$ mice was parallel to the rate of angiogenesis. However, there was no difference in angiogenic vessel permeability between *iNOS*-deficient mice and corresponding WT mice with immunocompetent C57BL/6 background (Table 1).

NO Level in VEGF Gel Is Decreased in *eNOS*$^{-/-}$*Rag-1*$^{-/-}$ Mice. Examples of individual NO profiles measured in VEGF gels in WT *Rag-1*$^{-/-}$ and *eNOS*$^{-/-}$*Rag-1*$^{-/-}$ (KO) mice are shown in Fig. 4 *A* and *B*, respectively. Spatial variations in NO were observed as the microsensor was advanced through the gels, which may be related to individual vessels and/or other NO-producing cells along the measurement track. Significantly elevated NO levels were observed in VEGF gels in WT *Rag-1*$^{-/-}$ mice compared with NO levels in normal brain tissue and in VEGF gels in *eNOS*$^{-/-}$*Rag-1*$^{-/-}$ mice. In WT *Rag-1*$^{-/-}$ mice, the peak NO level (2.01 ± 0.25 μM, $n = 6$) was observed at the bottom of the gel (375 ± 48 μm), close to the underlying pial surface, which is presumably the area with highest angiogenic activity in the gel. L-NIL treatment in WT *Rag-1*$^{-/-}$ mice did not reduce the peak NO level in the gel significantly (1.76 ± 0.36 μM at 342 ± 60 μm, $n = 3$, $P = 0.584$). As shown in Fig. 4*B* for an *eNOS*$^{-/-}$*Rag-1*$^{-/-}$ mouse, no NO peak was observed in the gel and the highest values were observed in brain tissue under the gel (depth greater than 400 μm). The average NO level near the bottom of the gel in *eNOS*$^{-/-}$*Rag-1*$^{-/-}$ mice (0.26 ± 0.04 μM at 425 μm, $n = 2$, $P = 0.019$) was significantly lower than the peak NO value in WT *Rag-1*$^{-/-}$ mice. Averaged NO profiles (data point for each 50-μm increment) demonstrate the pattern WT *Rag-1*$^{-/-}$ ≥ WT *Rag-1*$^{-/-}$ with L-NIL >> *eNOS*$^{-/-}$*Rag-1*$^{-/-}$ with and without L-NIL, with peak NO values for the WT *Rag-1*$^{-/-}$ mice significantly higher ($P = 0.008$) than NO levels at the bottom of the gel in *eNOS*$^{-/-}$*Rag-1*$^{-/-}$ mice (Fig. 4*C*). NO level was significantly reduced throughout the collagen gel in *eNOS*$^{-/-}$*Rag-1*$^{-/-}$ mice, and some effect of L-NIL on NO level was observed near the bottom of the gel where the host cell migration occurs.

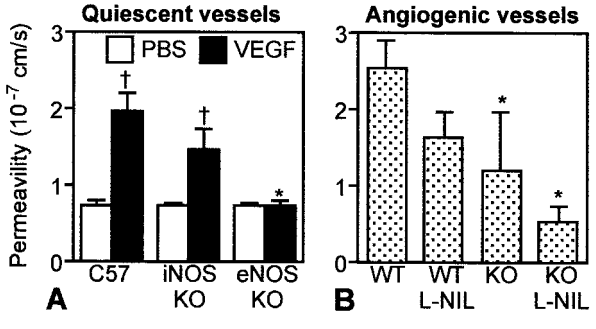

Fig. 3. VEGF-induced vascular permeability in quiescent and angiogenic vessels. Vascular permeability to BSA was determined by intravital microcopy in quiescent (*A*) and angiogenic (*B*) vessels. (*A*) VEGF superfusion significantly increased vascular permeability in C57BL/6 ($n = 4$) and *iNOS*$^{-/-}$ ($n = 3$) mice but not in *eNOS*$^{-/-}$ ($n = 3$) mice. (*B*) NOS inhibition in the VEGF gels (*Rag-1*$^{-/-}$ (WT) with L-NIL, *eNOS*$^{-/-}$*Rag-1*$^{-/-}$ (KO), KO with L-NIL) decreased permeability ($1.6 \pm 0.3 \times 10^{-7}$ cm/s, $n = 6$, $P = 0.0727$; $1.2 \pm 0.8 \times 10^{-7}$ cm/s, $n = 3$, $P = 0.035$; $0.5 \pm 0.2 \times 10^{-7}$ cm/s, $n = 3$, $P = 0.003$; respectively) compared with WT mice ($2.5 \pm 0.4 \times 10^{-7}$ cm/s, $n = 8$). †, $P < 0.05$ as compared with PBS treatment. *, $P < 0.05$ as compared with corresponding C57 or WT mice.

Discussion

VEGF Induces NO Production via eNOS. Vascular endothelial cells express high affinity VEGF receptors flt-1 and flk-1/KDR (2). During certain periods of development and under pathological conditions such as cancer, angiogenic blood vessels also express another VEGF receptor, flt-4 (23, 24), that is normally restricted to the lymphatic endothelium in adults. Among the three VEGF receptors, flk-1/KDR is believed to play the predominant role in angiogenesis (2). A recent study also has shown that flk-1/KDR mediates NO production induced by VEGF (25). VEGF stimulates formation of an flk-1/KDR–*c-src* complex, which triggers Ca^{2+} release through the IP_3 second messenger pathway. As a result, eNOS, which is Ca^{2+}-dependent and constitutively expressed in vascular endothelial cells, is almost immediately activated after tissue exposure to VEGF. Furthermore, it was recently reported that VEGF induces expression of eNOS in human umbilical vein endothelial cells and that activation of eNOS expression is regulated by protein kinase Akt (9–11, 26). Endothelial cell survival by VEGF is regulated through the flk-1/KDR and phosphoinositide 3-kinase/Akt signal transduction pathways (27). Thus, NO may be involved in VEGF-induced endothelial cell survival as well. VEGF induces NO production from vascular endothelial cells by increasing both NOS enzyme expression and activity *in vitro* (9–11). Thus, it is reasonable to assume that NO is produced from vascular endothelial cells via eNOS in response to VEGF *in vivo*. Indeed, in this study we found that gene deletion of *eNOS* results in significantly reduced NO levels in the VEGF containing gel.

eNOS Mediates VEGF-Induced Angiogenesis. VEGF induces vascular endothelial migration, proliferation, and capillary-like network formation *in vitro*, and vasculogenesis and angiogenesis *in vivo* (2). Addition of broad-spectrum NOS inhibitors blocks these VEGF functions *in vitro* (11, 13). Furthermore, systemic treatment with NOS inhibitors suppresses VEGF-induced angiogenesis *in vivo* (13). In agreement with a previous finding using an ischemic limb and wound repair models (28, 29), we find that *eNOS* null mice showed significantly reduced angiogenesis in both control and VEGF-containing collagen gels compared with corresponding WT mice. Furthermore, the rates of angiogenesis in control gel and VEGF gel were comparable in *eNOS* null mice. These results demonstrate that eNOS is the major NOS isoform mediating angiogenesis induced by VEGF *in vivo*.

Involvement of iNOS in VEGF-Induced Angiogenesis. In addition to vascular endothelial cells, other cell types express VEGF receptors. Monocytes express flt-1 and VEGF induces migration of these cells (30). Recently, another receptor, neuropilin-1 (NP-1) was found to bind to VEGF (31). In collaboration with flk-1/KDR, NP-1 enhances VEGF function in endothelial cells. Furthermore, NP-1 may mediate VEGF-induced changes in nonendothelial cells. We expect in our study that VEGF may induce migration of nonendothelial cells into the collagen gel. Thus, vascular endothelial cells may not be the only cell type in an angiogenic tissue. In fact, many nonendothelial cells infiltrated into the collagen gel in our study. Migrated host stromal cells such as macrophages and fibroblasts in wound, matrix implant, and tumor tissue also express angiogenic stimulators including VEGF and iNOS (32, 33). These cells may be exposed to hypoxia in the tissue. Hypoxia is known to induce several genes including VEGF and iNOS (34, 35). Furthermore, Kroll

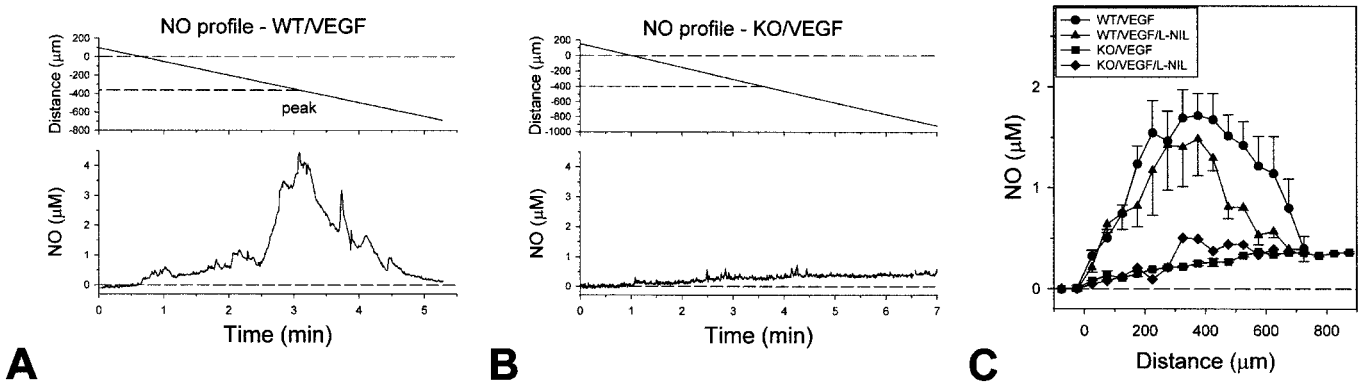

Fig. 4. NO concentration profiles across VEGF gels. Individual (*A* and *B*) and overall averaged (*C*) measurements of NO concentration profiles across VEGF gels and into the underlying brain tissue. (*A* and *B*) The position of the tip relative to the gel surface (*Upper*) and resulting NO measurement (*Lower*) as a function of time while the microsensor was advanced are shown for individual NO concentration profiles in VEGF gels implanted in a *Rag-1*$^{-/-}$ (WT) mouse (*A*) and an *eNOS*$^{-/-}$*Rag-1*$^{-/-}$ (KO) mouse (*B*). The peak NO value for this WT mouse ($>$ 4 μM) was located at -362 μm (below the gel surface), near the bottom of the gel. There was no noticeable NO peak in the gel for the KO measurement in the range from 0 to -400 μm. (*C*) NO profiles averaged over 50 μm increments for a total of 29 profiles in six WT mice, 19 profiles in three L-NIL treated WT mice, 11 profiles in two KO mice, and one profile in one L-NIL-treated KO mouse. Averaged NO profiles demonstrate the pattern WT $>$ WT with L-NIL $\gg$ KO with and without L-NIL.

and Waltenberger (10) showed that activation of Flk-1/KDR leads to an up-regulation of not only eNOS but also iNOS protein in human umbilical vein endothelial cells. Thus, iNOS is potentially present and involved in VEGF-induced angiogenesis. Indeed, we found iNOS expression in the collagen gel, although the expression level is variable and significantly lower than eNOS (see Fig. 6, which is published as supplemental material). Because iNOS is Ca^{2+}-calmodulin independent and has an order of magnitude higher NO productivity compared with constitutive isoforms such as eNOS and nNOS, its lower expression level does not necessarily imply negligible biological function. In fact, both the iNOS selective inhibitor and *iNOS* gene deletion slowed angiogenesis in VEGF-containing gels, although it was less effective than *eNOS* gene deletion. We might potentially underestimate the relative contribution of iNOS when we use immunodeficient mice. However, the magnitude of response to iNOS inhibitor in immunodeficient mice and *iNOS* gene deletion in immunocompetent mice was similar. Furthermore, angiogenesis in VEGF gel in WT and *Rag-1*$^{-/-}$ mice with the same strain background (C57BL/6) was comparable (see Fig. 7, which is published as supplemental material). Nevertheless, it is noteworthy that treatment of *eNOS*$^{-/-}$*Rag-1*$^{-/-}$ mice with L-NIL led to a more significant delay in angiogenesis in the VEGF gel, suggesting that eNOS and iNOS play additive and/or complementary roles in angiogenesis. In summary, our angiogenesis assay suggests that there is a role for iNOS in VEGF-induced angiogenesis as well.

NO Mediates Hemodynamics in VEGF-Induced Angiogenic Vessels. The first host tissue response to an angiogenic stimulus from implanted tumor xenografts or growth factors is host vessel dilatation. NO was originally discovered as an endothelium-derived relaxing factor and is known to be a potent vasodilator (3, 36, 37). NO dilates host vessels, causing sprout formation, and maintains blood flow in angiogenic vessels (18, 38). In this study, functional vessel density, diameter and blood flow rate in the VEGF gels were reduced in *eNOS* mutant mice and to a lesser extent in iNOS inhibitor-treated mice or *iNOS*-deficient mice compared with corresponding WT mice. Pial vessel diameter in *eNOS*$^{-/-}$ mice was significantly smaller than that in WT C57 mice with comparable centerline velocity (see Fig. 8, which is published as supplemental material). These findings suggest that eNOS in the connecting host vessel regulates its vessel diameter and thus, is also important for angiogenesis and hemodynamics in angiogenic vessels. Hemodynamics in angiogenic vessels are regulated by both existing host vessels and angiogenic vessels themselves. Increased perfusion in VEGF-induced angiogenic vessels was mediated by NO-induced vasodilation (39).

eNOS Mediates VEGF-Induced Permeability. VEGF is known to increase vascular permeability of microvessels to circulating macromolecules (1). Increased vascular permeability often is observed in areas of pathological angiogenesis in solid tumors, wounds, and chronic inflammation. Indeed, extravasated plasma proteins form a fibrin-rich matrix suitable for angiogenic vessels to migrate/proliferate into. NO also mediates vascular permeability, although the effect of NO on vascular permeability seems to be context-dependent. In tumors or in chronic inflammation, NO enhances vascular permeability (5, 18). On the other hand, in some ischemia-reperfusion injury models, NO maintains vessel integrity (40). Nevertheless, studies using *ex vivo* perfused porcine coronary venules, the rat Miles assay and the rat cranial window have shown that VEGF enhances vascular permeability, whereas nonselective NOS inhibitors attenuate this effect (12, 41, 42). We found that the vascular permeability of both quiescent vessels acutely exposed to VEGF and angiogenic vessels induced by VEGF was significantly lower in *eNOS* null mice than that in WT control mice. On the other hand, VEGF increased vascular permeability in both quiescent and angiogenic vessels to a similar extent in *iNOS* null mice and WT C57 mice, although addition of iNOS inhibitor tended to decrease vascular permeability in angiogenic vessels. These results indicate that VEGF-induced vascular hyperpermeability is predominantly mediated by eNOS.

In this study, we could not detect nNOS mRNA in the VEGF containing gels by reverse transcriptase–PCR using a forward primer specific to exon 1 and a reverse primer specific to exon 2 (see Fig. 6). Although in principle, the exon 2-containing form of nNOS accounts for the majority of nNOS catalytic activity in the brain, there are several spliced variants of nNOS mRNA lacking exon 2 (43). Thus, although we do not have evidence that nNOS is significantly involved in angiogenesis in our system, we cannot exclude the possible involvement of alternatively spliced variants of nNOS in angiogenesis.

VEGF induces proangiogenic changes such as vessel dilatation, increased vascular permeability, and angiogenesis *in vivo* in tissues of adult mice. NO mediates these processes predominantly via eNOS. NO produced by iNOS also modifies both

angiogenesis and vascular permeability but to a lesser degree than eNOS. Unlike VEGF mutant mice, none of the NOS isoform mutant mice are embryonic lethal and grow relatively well, whereas wound repair is impaired in adult *eNOS* or *iNOS* mutant mice (29, 44). NO may be involved in pathological angiogenesis such as that occurring in solid tumors, but may not be essential for physiological angiogenesis such as occurring in development and vasculogenesis. Relative contributions of the NOS isoforms in angiogenesis and/or vascular permeability may depend on tissue, stimuli, and type of pathology.

Conclusions

NO modulates VEGF-induced angiogenesis and vascular permeability *in vivo*. Endothelial NOS predominantly mediates this process, and iNOS appears to have a small but additive effect. Thus, selective modulation of eNOS activity is a promising strategy for altering angiogenesis and vascular permeability *in vivo*.

We thank Attila Fabian, Amy Buikeine, Feng Zhou, and Amy Alt for genotyping, breeding, and maintenance of mice, Dr. Carla Mouta Carreira for her helpful comments, and Drs. Lei Xu and Emmanuelle di Tomaso for molecular evaluation. This study was supported in part by grants from the Alexander and Margaret Stewart Trust (D.F.), The Japan Health Sciences Foundation (Y.I.), and Grants R35-CA56591, R24-CA85140 (R.K.J.), NS33335, HL57818 (P.L.H.), and EY09269 (D.G.B.) from the National Institutes of Health (Bethesda, MD). P.L.H. is an Established Investigator of the American Heart Association.

1. Carmeliet, P. & Jain, R. K. (2000) *Nature (London)* **407,** 249–257.
2. Ferrara, N. (1999) *Kidney Int.* **56,** 794–814.
3. Ignarro, L. J., Cirino, G., Casini, A. & Napoli, C. (1999) *J. Cardiovasc. Pharmacol.* **34,** 879–886.
4. Bertuglia, S., Colantuoni, A. & Intaglietta, M. (1994) *Microvasc. Res.* **48,** 68–84.
5. Fukumura, D. & Jain, R. K. (1998) *Cancer Metastasis Rev.* **17,** 77–89.
6. Xie, K., Dong, Z. & Fidler, I. J. (1996) *J. Leukocyte Biol.* **59,** 797–803.
7. De Caterina, R., Libby, P., Peng, H. B., Thannickal, V. J., Rajavashisth, T. B., Gimbrone, M. A. J., Shin, W. S. & Liao, J. K. (1995) *J. Clin. Invest.* **96,** 60–68.
8. Nathan, C. & Xie, Q.-W. (1994) *Cell* **78,** 915–918.
9. Hood, J. D., Meininger, C. J., Ziche, M. & Granger, H. J. (1998) *Am. J. Physiol.* **274,** H1054–H1058.
10. Kroll, J. & Waltenberger, J. (1998) *Biochem. Biophys. Res. Commun.* **252,** 743–746.
11. Papapetropoulos, A., Garcia-Cardena, G., Madri, J. A. & Sessa, W. C. (1997) *J. Clin. Invest.* **100,** 3131–3139.
12. Murohara, T., Horovitz, J. R., Silver, M., Tsurumi, Y., Chen, D., Sullivan, A. & Isner, J. M. (1998) *Circulation* **97,** 99–107.
13. Ziche, M., Morbidelli, L., Choudhuri, R., Zhang, H. T., Donnini, S., Granger, H. J. & Bichnell, R. (1997) *J. Clin. Invest.* **99,** 2625–2634.
14. Huang, P. L., Huang, Z., Mashimo, H., Block, K. D., Moskowitz, M. A., Beven, J. A. & Fishman, M. C. (1995) *Nature (London)* **377,** 239–242.
15. Mombaerts, P., Iccomini, J., Johnson, R. S., Herrup, K., Tonegawa, S. & Papaioannou, V. E. (1992) *Cell* **68,** 869–877.
16. Dellian, M., Witwer, B. P., Salehi, H. A., Yuan, F. & Jain, R. K. (1996) *Am. J. Pathol.* **149,** 59–72.
17. Gohongi, T., Fukumura, D., Boucher, Y., Yun, C.-O., Soff, G. A., Compton, C., Todoroki, T. & Jain, R. K. (1999) *Nat. Med.* **5,** 1203–1208.
18. Fukumura, D., Yuan, F., Endo, M. & Jain, R. K. (1997) *Am. J. Pathol.* **150,** 713–725.
19. Stenger, S., Donhauser, N., Thuring, H., Rollinghoff, M. & Bogdan, C. (1996) *J. Exp. Med.* **183,** 1501–1514.
20. Moore, W. M., Webber, R. K., Jerome, G. M., Tjoeng, F. S., Misko, T. P. & Currie, M. G. (1994) *J. Med. Chem.* **37,** 3886–3888.
21. Monsky, W. L., Fukumura, D., Gohongi, T., Ancukiewcz, M., Weich, H. A., Torchilin, V. P., Yuan, F. & Jain, R. K. (1999) *Cancer Res.* **59,** 4129–4135.
22. Buerk, D. G., Riva, C. E. & Cranstoun, S. D. (1996) *Microvasc. Res.* **52,** 13–26.
23. Dumont, D. J., Jussila, L., Taipale, J., Lymboussaki, A., Mustonen, T., Pajusola, K., Breitman, M. & Alitaro, K. (1998) *Science* **282,** 946–949.
24. Valtola, R., Salven, P., Heikkila, P., Taipale, J., Joensun, H., Rehn, M., Pihlajaniemi, T., Weich, H., deWaal, R. & Alitaro, K. (1999) *Am. J. Pathol.* **154,** 1381–1390.
25. He, H., Venema, V. J., Gu, X., Venema, R. C., Marrero, M. B. & Caldwell, R. B. (1999) *J. Biol. Chem.* **274,** 25130–25135.
26. Fulton, D., Gratton, J.-P., McCabe, T. J., Fontana, J., Fujio, Y., Walsh, K., Franke, T. F., Papapetropoulos, A. & Sessa, W. C. (1999) *Nature (London)* **399,** 597–601.
27. Gerber, H. P., McMurtrey, A., Kowalski, J., Yan, M., Keyt, A., Dixit, V. & Ferrara, N. (1998) *J. Biol. Chem.* **273,** 30336–30343.
28. Murohara, T., Asahara, T., Silver, M., Bauters, C., Masuda, H., Kalka, C., Kearney, M., Chen, D., Symes, J. F., Fishman, M. C., *et al*. (1998) *J. Clin. Invest.* **101,** 2567–2578.
29. Lee, P. C., Salayapongse, A. N., Bragdon, G. A., Shears, L. L., II, Watkins, S. C., Edington, H. D. J. & Billiar, T. R. (1999) *Am. J. Physiol.* **277,** H1600–H1608.
30. Barleon, B., Sozzani, S., Zhou, D., Weich, H. A., Mantoani, A. & Marmé, D. (1996) *Blood* **87,** 3336–3343.
31. Soker, S., Takashima, S., Miao, H.-Q., Neufeld, G. & Klagsbrun, M. (1998) *Cell* **92,** 735–745.
32. Fukumura, D., Xavier, R., Sugiura, T., Chen, Y., Park, E., Lu, N., Selig, M., Nielsen, G., Taksir, T., Jain, R. K. & Seed, B. (1998) *Cell* **94,** 715–725.
33. Montrucchio, G., Lupia, E., De Martino, A., Battaglia, E., Arese, M., Tizzani, A., Bussolino, F. & Camussi, G. (1997) *Am. J. Pathol.* **151,** 557–563.
34. Melillo, G., Musso, T., Sica, A., Taylor, L. S., Cox, G. W. & Varesio, L. (1995) *J. Exp. Med.* **182,** 1683–1693.
35. Shweiki, D., Itin, A., Soffer, D. & Keshet, E. (1992) *Nature (London)* **359,** 843–845.
36. Furchgott, R. F. & Zawadzki, J. V. (1980) *Nature (London)* **288,** 373–376.
37. Palmer, R. M., Ferrige, A. G. & Moncada, S. (1987) *Nature (London)* **327,** 524–526.
38. Carmeliet, P. (2000) *Nat. Med.* **6,** 389–395.
39. García-Cardeña, G. & Folkman, J. (1998) *J. Natl. Cancer Inst.* **90,** 560–561.
40. Kubes, P. & Granger, D. (1992) *Am. J. Physiol.* **262,** H611–H615.
41. Mayhan, W. G. (1999) *Am. J. Physiol.* **276,** C1148–C1153.
42. Wu, H. M., Huang, Q., Yuan, Y. & Granger, H. J. (1996) *Am. J. Physiol.* **271,** H2735–H2739.
43. Eliasson, M. J., Blackshaw, S., Schell, M. J. & Snyder, S. H. (1997) *Proc. Natl. Acad. Sci. USA* **94,** 3396–3401.
44. Yamasaki, K., Edington, H. D. J., McClosky, C., Tzeng, E., Lizonova, A., Kovesdi, I., Steed, D. L. & Billiar, T. R. (1998) *J. Clin. Invest.* **101,** 967–971.